

N-containing functional groups induced superior cytocompatible and hemocompatible graphene by NH₂ ion implantation

Meixian Guo · Minsi Li · Xiaoqi Liu · Mengli Zhao ·
Dejun Li · Dongsheng Geng · Xueliang Sun ·
Hanqing Gu

Received: 29 January 2013 / Accepted: 22 July 2013 / Published online: 2 August 2013
© Springer Science+Business Media New York 2013

Abstract Graphene is functionalized with amine by NH₂ ion implantation at room temperature in vacuum. The reaction is featured by nucleophilic substitution of C–O groups by the ammonia radicals. The presence of N-containing functional groups in graphene is identified by Fourier transform infrared spectroscopy and X-ray photoelectron spectroscopy. N element was successfully introduced to graphene, the atomic ratio of N to C rose to 3.12 %. NH₂ ion implanted graphene (G-NH₂) is a better hydrophilic material than pristine graphene according to the contact angle experiment. Mouse fibroblast cells and human endothelial cells cultured on G-NH₂ displayed superior cell-viability, proliferation and stretching over that on pristine graphene. Platelet adhesion, hemolysis and Kinetic-clotting time were measured on G-NH₂, showing excellent anticoagulation, with as good hemolysis as pristine graphene.

M. Guo · X. Liu · M. Zhao · D. Li (✉)
College of Physics and Electronic Information Science, Tianjin
Normal University, Tianjin 300387, China
e-mail: dejunli@mail.tjnu.edu.cn

M. Li
School of Chemistry and Materials Science, University of
Science and Technology of China, Hefei 230026, China

D. Geng · X. Sun
Department of Mechanical & Materials Engineering, University
of Western Ontario, London, ON N5X 4J6, Canada

H. Gu
Tianjin Institute of Urological Surgery, Tianjin Medical
University, Tianjin 300070, China

H. Gu
Ninth People's Hospital, School of Medicine, Shanghai Jiao
Tong University, Shanghai 200011, China

1 Introduction

In recent years, a lot of engineered nanomaterials such as carbon nanotubes are fabricated, investigated for their effects on the cells, animals and environment, and evaluated for their biosafety [1–5]. Unlike other carbon-based nanomaterials, biomedical applications of graphene have grown at a rapid pace and exhibit immense potential for the future. Graphene-based materials are of great interest due to its remarkable physical, chemical, and biological characteristics. The distinct structural properties of graphene, in particular, its high aspect ratio, unique electronic and optical properties, high mechanical strength, as well as potential biocompatibility, render it an attractive candidate for a plethora of applications in biotechnology including biosensor development, drug delivery, bacterial inhibition, photothermal therapy, and electrical stimulation of cells [6–14]. Thanks to the biocompatibility at low concentration [15] and 2D nature with ultra-large surface area, graphene and graphene oxide (GO) have recently captured interests as cell culture substrates. Substrates coated with graphene or GO have enabled the culture of several mammalian cells including NIH-3T3 [16] and A549 [17], but the widespread use of graphene and GO for cell culture necessitates more intensive research.

For biomedical and pharmaceutical applications, it is extremely important that graphene preparation should be biocompatible, water-dispersible, and nontoxic. These attributes are achievable by appropriate chemical functionalization, which enables graphene to be well-dispersed in a range of polar solvents and particularly well in water [18, 19]. Nitrogen is a common heteroatom which can be introduced into carbon nanomaterials by thermal treatment of carbon in the presence of nitrogen precursors, by *in situ* growth or by chemical vapor deposition. N-doped carbon

show improved catalytic and electrochemical performances [20–26]. However, substituted nitrogen gives poor wettability and chemical reactivity, which need to be improved by further chemical modification. Unlike nitrogen substitution, primary amine can be introduced into graphene as ionizable functional groups which could form cations or cationic groups. These ionizable groups could not only improve the solubility of graphene, but also facilitate graphene assembly or reaction with other organic molecules, polymers and biological systems [27]. It has been proven that for biomedical applications, chemical functionalization of amine-modified graphene displays safer trombo-protective behaviour than graphene oxide [28].

Ion implantation is one of the most powerful physical techniques for the surface modification of solids. This technique has many advantages in applications. Apart from the technological simplicity and cleanliness, it modifies only the surface characteristics without affecting bulk properties [29]. It has been applied to the surface modification of polymers in order to control to conductive, mechanical, physical and chemical properties [30–34]. Therefore, if biomaterials with the desired bulk properties do not exhibit the appropriate biocompatibility, their surface can be modified by this technique. This encourages us to search for alternative chemical derivatives of graphene with similar physical attributes, which have minimal or low thrombogenic potential and better cytocompatibility. To date, amine-functionalized graphene by ion implantation has not been studied for biomedical applications, while amine-modified single-walled carbon nanotubes are recently shown to be cytoprotective toward neuronal cells [35, 36]. Here we report that positively charged NH₂ ion implanted graphene (G-NH₂) is more biocompatibility than graphene.

2 Methods

2.1 Sample preparation and characteristic analysis

Graphene powder prepared by modified Hummers' method was dissolved in 1-methyl-2-pyrrolidinone (NMP) with ultrasonic dispersion for 6 h [37], then the solution was directly sprayed onto the cycloidal SiO₂ substrate using air brush pistol at 100 °C. Finally, the samples were heated in Ar at 250 °C for 3 h to evaporate the NMP. NH₂ ion implantation on graphene surface was performed at energy of 30 keV at room temperature using the BNU-400 kV Implanter. The ion fluency was 5×10^{14} and 1×10^{16} ions/cm².

Static (sessile drop) water contact angle (CA) on pristine graphene and G-NH₂ were determined with the CAM KSV021733 optical contact-angle inclinometer (Nunc,

Finland). High-resolution transmission electron microscopy (HR-TEM) studies were performed to examine crystallinity and quality of pristine graphene and G-NH₂. The functional groups for G-NH₂ were analyzed by MAGNA-560 typed Fourier transformer infrared (FTIR) spectrophotometer (Nicolet) and Kratos Axis Ultra Al (alpha) X-ray photoelectron spectroscopy (XPS).

2.2 Cell adhesion assays

Cell mortality of mouse fibroblast cells (L929) and human umbilical vein endothelial cells (EAHY 926) were investigated by trypan blue assay. L929 cells were incubated at 37 °C in a 5 % CO₂ atmosphere in Roswell Park Memorial Institute-1640 medium supplemented with heat inactivated 10 % fetal bovine serum, 100 U/ml penicillin and 100 µg/ml streptomycin. EAHY926 cells were cultured in Dulbecco's Modified Eagle Medium/High Glucose supplemented with 10 % fetal bovine serum, 100 units/ml penicillin and 100 µg/ml streptomycin, in a humidified 5 % CO₂ balanced air incubator at 37 °C. Medium was changed every 2 days. The cells were passed with 0.25 % trypsin plus 0.02 % EDTA.

Both the cells were plated in 24-well culture plates with sterilized samples at a concentration of 5×10^4 cells/ml for EAHY926 and 1×10^4 cells/ml for L929 in individual wells. After incubated for 1, 1.5, 2, 3, 5 and 7 days, alive and dead cell numbers were counted using trypan blue dye assay in order to confirm the viability of cells. Cell morphology and stretching on pristine graphene and G-NH₂ was observed through scanning electron microscope (SEM, FEI QUANTA 200).

2.3 Platelet-adhesion assays

Platelet-adhesion testing was performed to investigate the morphology, quantity and aggregation of the adherent platelets on the surface of samples. All the samples were placed in individual wells of 24-well culture plate. Fresh blood from healthy rabbit with potassium oxalate as the anticoagulant was centrifuged at 1000 rpm for 10 min to prepare platelets rich plasma (PRP). A total of 600 µl of PRP was added into each well and incubated at 37 °C for 30 min under static conditions. After being rinsed with PBS, the substrates were immersed in glutaraldehyde in PBS 30 min and critical-point dried under vacuum. Finally, the samples were observed using a SEM after coating with gold. Three different spots were observed on each sample.

2.4 Hemolysis assays

Fresh anticoagulated blood from healthy rabbit was diluted with 10 ml of normal saline solution (with concentration of

0.9 %) at the volume ratio of 4:5. The pristine graphene and G-NH₂ were washed three times by normal saline and immersed into 5 ml normal saline. 0.1 ml diluted blood was successively added into the solution of all groups, gently shaken for uniformity and kept in water bath at 37 ± 1 °C for 60 min. The liquid was removed by centrifugation at rotational speed of 1000 rpm for 10 min. The absorbance value of supernatant was measured at wavelength of 545 nm with a spectrophotometer. The mean value of three measurements was calculated. Positive control group consisted of 0.1 ml diluted blood in 5 ml tri-distilled water while negative control group consisted of 0.1 ml diluted blood in 5 ml normal saline solution. The optical density (O.D.) was related to the concentration of free hemoglobin in the supernatant due to broken red blood cells. Hemolysis degree was calculated as:

$$\text{Hemolytic rate (\%)} = \frac{A - B}{C - B} \times 100 \%$$

where A is the absorbance of samples; B and C are the absorbance of the negative and positive groups. According to the YY/T0127.1 standard, a hemolytic rate below 5 % is acceptable in clinical.

2.5 Kinetic blood-clotting time assays

0.1 ml fresh blood taken from a healthy adult rabbit was dropped onto the surface of the samples. After being kept for 5, 10, 20, 30, 40, 50 min respectively, the samples were transferred into a beaker with 50 ml distilled water. Then the escaped erythrocytes from thrombus were hemolytic, and the freed hemoglobin was dispersed in the solution. The concentration of freed hemoglobin in the solution was colorimetric analyzed by a spectrophotometer at the

wavelength of 540 nm. The optical density at 540 nm (O.D._{540 nm}) of the solution vs. time was plotted. In general, the O.D._{540 nm} value decreases with blood clotting.

3 Results and discussion

3.1 Characterization of graphene systems

The TEM images in Fig. 1 reveal that compared with pristine graphene, G-NH₂ consists of randomly aggregated thin sheets that are closely associated, forming a porous and disordered network. It is obviously that G-NH₂ with the fluency of 1×10^{16} ions/cm² is more porous than G-NH₂ with 5×10^{14} ions/cm². This suggests that G-NH₂ could be well dispersed in water and N methyl pyrrolidone (NMP) with better solubility than pristine graphene, which is consistent with the contact angle (CA) of substrates evaluated by the sessile drop method (inset of Fig. 1). The CA value reduces to 58.58° for G-NH₂ from 89.54° for pristine graphene, and decreases with fluency increasing. The polydispersibility of G-NH₂ in water and several organic solvents should be related to the hydrophilicity of N-containing functional groups, which makes G-NH₂ an ideal candidate for biomedical applications. Hydrophilic surface promotes fibronectin adsorption which is consistent with cell proliferation, migration, differentiation and apoptosis. Nonwetting substrates with low surface energies have been reported to result in protein denaturation, exposing the inner hydrophobic residues of proteins and preventing specific interactions between the adsorbed protein and cells [38, 39].

The FTIR spectra of pristine graphene and G-NH₂ (Fig. 2a) demonstrate the presence of C=C (V_{C-C} at

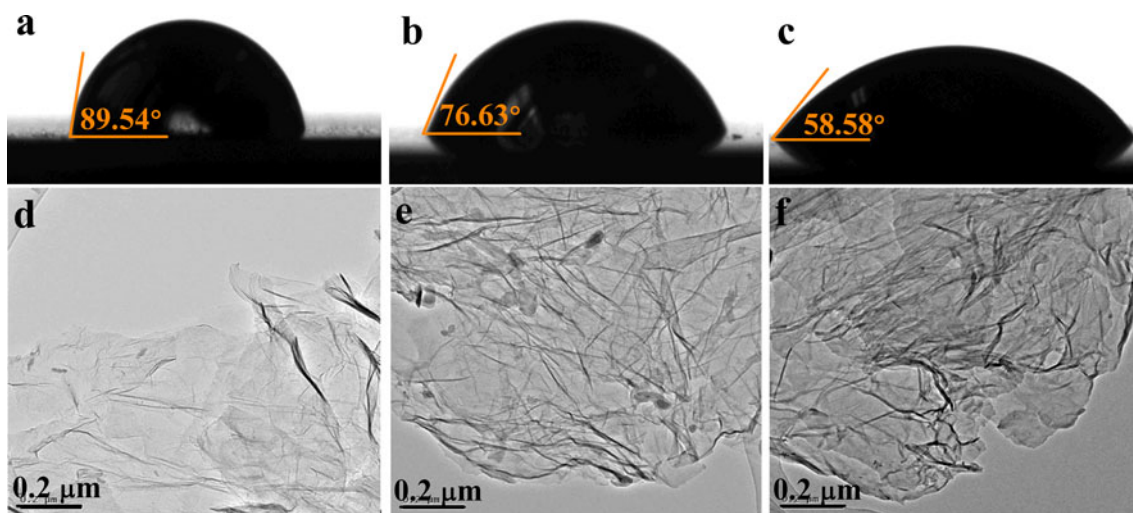


Fig. 1 Water contact angle images of pristine graphene (a), G-NH₂ with fluency of 5×10^{14} (b) and 1×10^{16} ions/cm² (c); TEM images of pristine graphene (d), G-NH₂ with fluency of 5×10^{14} (e) and 1×10^{16} ions/cm² (f)

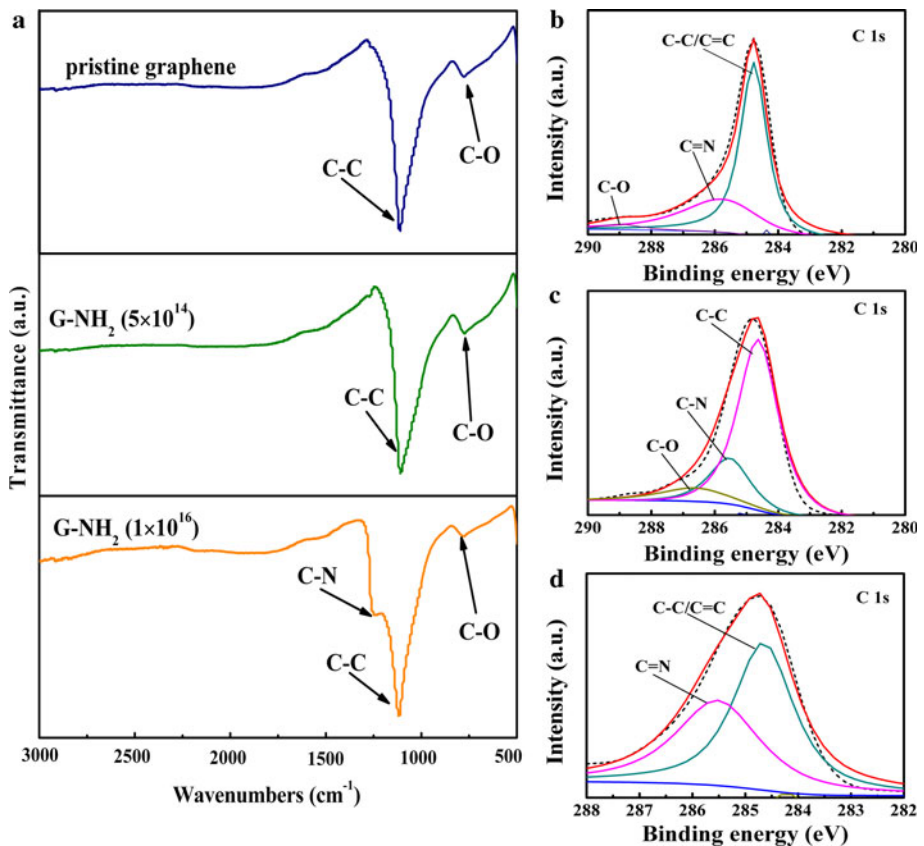
1111 cm^{-1}) and C–O ($V_{\text{C}-\text{O}}$ at 778 cm^{-1}). When the fluency is $5 \times 10^{14}\text{ ions/cm}^2$, there is no change from the FTIR spectra for G-NH₂. As the fluency increase to $1 \times 10^{16}\text{ ions/cm}^2$, there appears a new band at 1258 cm^{-1} , corresponding to C–N in-plane stretching, which may be attributed to the successful introduction of nitrogen by NH₂ ion implantation. XPS was performed to analyze both the chemical state and atomic ratio of each element in pristine graphene and G-NH₂ (Fig. 2b–d). The survey XPS spectra of G-NH₂ show intensified nitrogen peak at 285.5 eV and decreased oxygen peak at 286.7 eV as compared to that of pristine graphene, so far as to the oxygen peak disappears at $1 \times 10^{16}\text{ ions/cm}^2$. The atomic ratio of C: O for G-NH₂ is ~ 10.9 , which is much higher than that of pristine graphene (~ 4.8). The increase of C to oxygen atomic ratio indicates the de-oxygenation or reduction of graphene during the NH₂ ion implantation. More importantly, the XPS study shows that the molar ratio of carbon to nitrogen could be enhanced by NH₂ ion implantation, and the increase of the C=N peak intensity with the increase of the ion implantation dosage.

3.2 Cell viability and morphology

This assay is based on the principle of dye exclusion to differentiate between living, and dead cells. Living cells

with intact cell membranes prevent the trypan blue dye from entering them. Whereas, dead cells with compromised leaky cell membranes allow the dye to pass through. This allows dead cells stained by the dye to be visualized under an optical microscope. Figure 3a, b shows L929 cell and EAHY926 cell mean numbers on the surface of samples with incubation days. Each value in this figure represents the mean \pm SD for five measurements. Each experiment is performed three times. It is clearly that the cell concentrations on pristine graphene increase gradually despite lower cell adhesion originally. 5 days latter, a large number of dead cells appear, which lead L929 cell growth curve to decline gradually and EAHY926 cells almost stop proliferation. However, the cell concentration on G-NH₂ sustains increasing from 1 to 7 days, and exceeds that on pristine graphene at 7 days, especially for EAHY926 cells. L929 cells adhered on G-NH₂ with fluency of $1 \times 10^{16}\text{ ions/cm}^2$ has the largest numbers and fastest growth trend. EAHY926 cell on G-NH₂ at $1 \times 10^{16}\text{ ions/cm}^2$ maintains rapid growth trend despite lower numbers, while EAHY926 cell growth line of G-NH₂ with fluency of $5 \times 10^{14}\text{ ions/cm}^2$ is on a declining curve, indicating that graphene provides a better growth environment for cell viability after NH₂ ion implantation. From 1 to 3 days, no dead cells are observed under the optical microscope about all the samples. After incubated for 5 days, the percentage

Fig. 2 FTIR spectra obtained from pristine graphene and G-NH₂ with difference fluencies (a); XPS C1s spectra of pristine graphene (b), G-NH₂ with fluency of 5×10^{14} (c) and $1 \times 10^{16}\text{ ions/cm}^2$ (d)

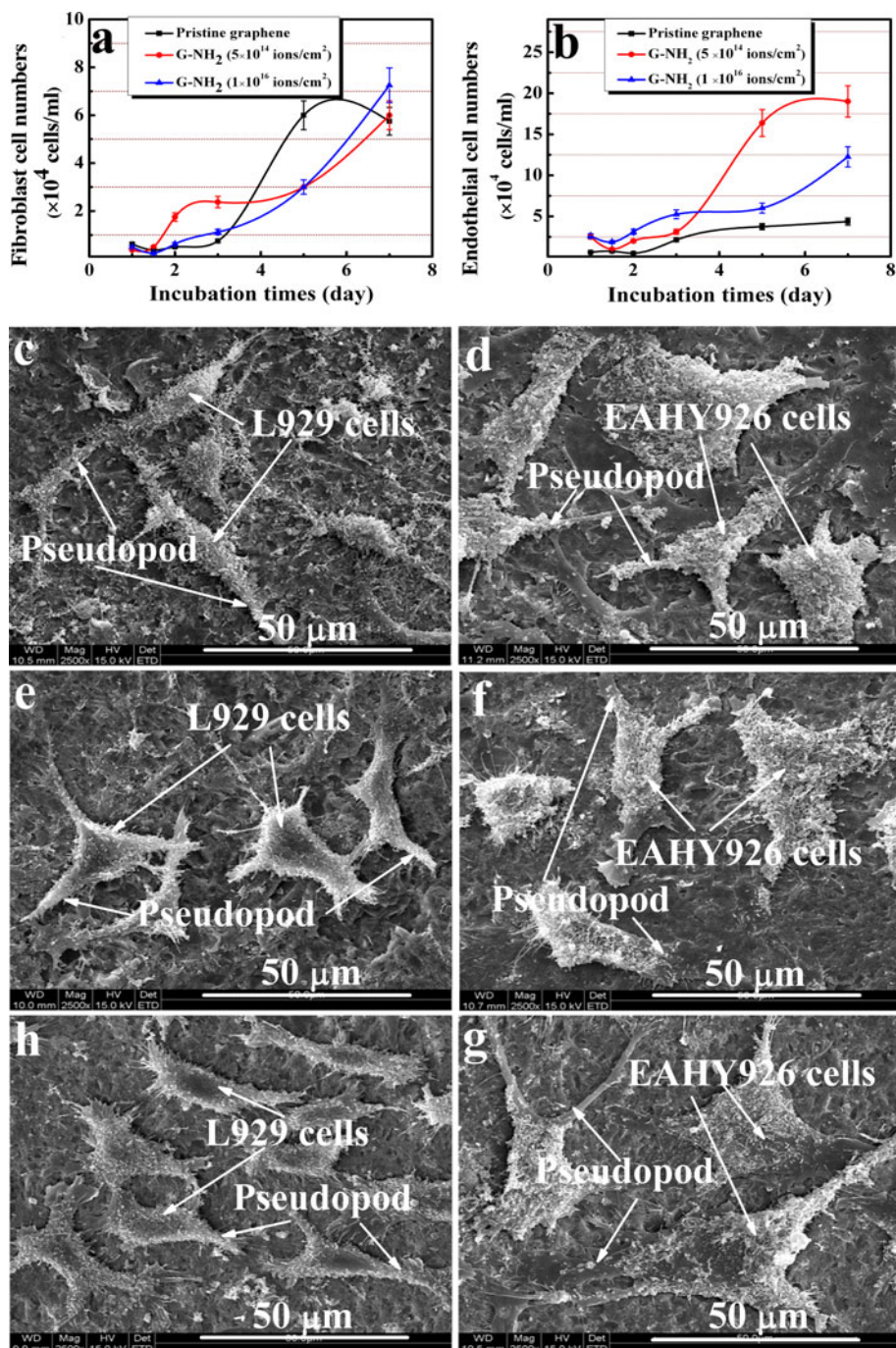


of the dead cell numbers from G-NH₂ is lower than 8 %, whereas the percentage of the dead cell numbers from pristine graphene is over 15 %. This indicates the significant contributions of nitrogen functional groups to cellular tissues and the voile-like structure consisting of randomly crumpled sheets, which offers a much larger substrate area for cell growth and proliferation.

Figure 3c–g shows the SEM images of L929 and EAHY926 cells adhered on the surfaces of graphene and

G-NH₂ after 3 days incubation. Compared with irregular, spindly cells on the surface of pristine graphene detach from culture plates and display morphological changes characteristic of apoptosis, typical aplanate cells adhered to the surface of G-NH₂ has the tendency to attach to the substrate and intersect with each other, what's more, the cells adhered on G-NH₂ with fluency of 1×10^{16} ions/cm² completely extend, indicating a significant improvement of cell adhesion. This result demonstrates that NH₂ ion

Fig. 3 L929 (a) and EAHY926 (b) cell numbers on different surfaces; SEM images of L929 cells on pristine graphene (c), G-NH₂ with fluency of 5×10^{14} (e) and 1×10^{16} ions/cm² (h), SEM images of EAHY926 cells on pristine graphene (d), G-NH₂ with fluency of 5×10^{14} (f) and 1×10^{16} ions/cm² (g)



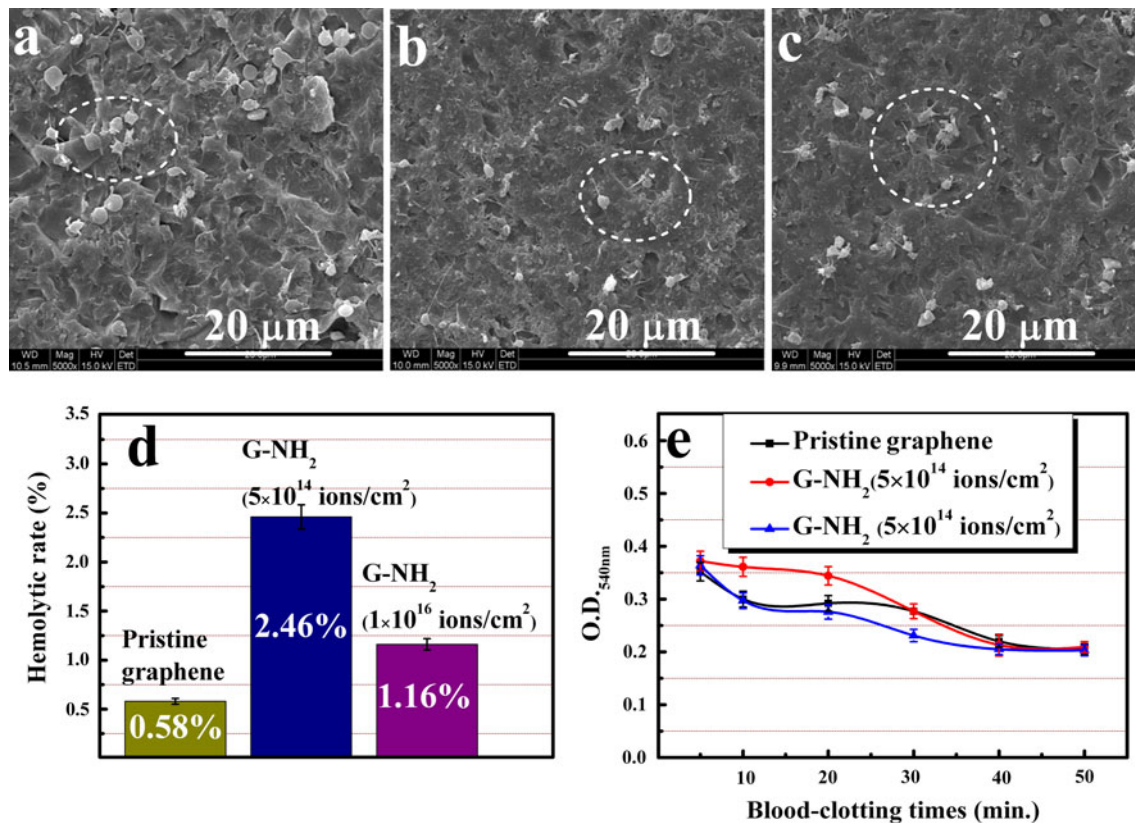


Fig. 4 SEM images of the platelets on pristine graphene (a), G-NH₂ with fluency of 5×10^{14} (b) and 1×10^{16} ions/cm² (c); Hemolytic rates (d) and O.D._{540 nm} values versus blood-clotting time (e) of different samples

implanted graphene can provide a proper surface for normal cellular growth. This is possibly because non-specific binding between nitrogen in the functionalized graphene and cell-surface proteins enhances cell adhesion and growth [40]. Surface chemistry as well as topographical parameters such as roughness and texture can affect surface wettability and the proliferation of cells because the initial phase of attachment involves the physicochemical linkages between cells and surfaces through interfaces or indirectly through an alteration in the adsorption of conditioning molecules e.g. proteins [41]. Surface charge distribution is another important regulator of the physical interface between nanomaterials and biological system. There have been recent reports suggestive of a correlation between the degree of functionalization or defects on carbon-based nanomaterials and ensuing cytotoxicity [42–44]. As direct interaction between nanomaterials and cells modulates critical cell signaling pathways and contributes to observed toxicity, positively charged modification of G-NH₂ induced by NH₂ ion implantation with ensuing diminished effect on nanomaterial-cell interaction can bring about significant attenuation in toxicity.

3.3 Platelet adhesion, hemolysis, and kinetic-clotting time

Platelet adhesion is one of the intuitive methods to measure the blood compatibility of biomaterials. Figure 4a–c clearly show the SEM images of platelet adhesion on different substrates. As expected, there are a lot of platelets adhering and aggregating with extended pseudopodia on the pristine graphene. However, when the NH₂ ions are implanted on the graphene with different fluencies, there are only a few platelets adhered on the G-NH₂ although they have similar deformation and activation to ones on pristine graphene. Compared with the pristine graphene, although the G-NH₂ surfaces may not support significant platelet adhesion, they could potentially still activate platelets. Platelets undergo a dramatic change in shape upon activation, platelet–platelet contact and adhesion are promoted, leading to the release of their intracellular granular contents, including P-selectin. Platelet pseudopodium and aggregation are marks of platelet activation and are considered to be a major mechanism of thrombosis [45]. We infer that, despite sharing strikingly similar structural morphology with pristine graphene, G-NH₂ at

different fluencies does not induce platelets adhesion, and has low demonstrable thrombogenicity.

Hemolysis is a common test for evaluating blood compatibility of biomaterials. All samples, with lower hemolysis degree compared to the YY/T0127.1 standard 5 %, can be considered nonhemolytic. Figure 4d shows the hemolytic-rate results of pristine graphene and G-NH₂. It is clearly that both G-NH₂ show higher hemolytic-rate than pristine graphene. However, hemolytic-rate of G-NH₂ decreases from 2.46 % at 5×10^{14} ions/cm² to 1.16 % at 1×10^{16} ions/cm². All materials have the hemolytic rate far lower than acceptable value of 5 %, indicating that graphene before and after functionalization is nonhemolytic. There are some potential reasons why NH₂ ion implantation induces an increase in hemolytic-rate of graphene. The radiation damage of graphene by NH₂ ion implantation leads to the formation of some defects on the surface, which is easy to cause red blood cell aberration, increasing hemolytic-rate. Compared with lower fluency, higher fluency of 1×10^{16} ions/cm² results in hemolytic-rate of fall. This is because that appearance of more N-containing functional groups on the surface of G-NH₂ with higher fluency, protecting red blood cells against being broken and releasing hemoglobin, leading to a decrease in hemolytic-rate. The O.D. of the hemolyzed hemoglobin solution changes with time. Higher O.D. value corresponds to better thromboresistance. When the blood is completely clotted on the samples, the O.D._{540 nm} value of the solution decreases to a steady range. Generally, blood starts to clot at 0.1 point of O.D._{540 nm} value at which the kinetic blood-clotting time on the sample surfaces is recorded. From Fig. 4e we can see that the clotting time of pristine graphene and G-NH₂ are longer than 50 min, revealing excellent hemocompatibility. Therefore, G-NH₂ can be used as an antithrombogenic material.

4 Conclusions

This work demonstrated, for the first time, graphene could be functionalized with NH₂ ion implantation. The presence of N-containing functional groups in graphene has been identified by FTIR, and XPS. The resulting G-NH₂ performed better cytocompatibility than pristine graphene. L929 cells and EAHY926 cells cultured on G-NH₂ displayed higher cell-viability, proliferation, and stretching compared with pristine graphene. The Low platelet adhesion, the acceptable hemolytic rate (below 5 %), and prolonged kinetic blood-clotting time were also observed on G-NH₂. These results demonstrated G-NH₂ is a better biomedical material with promising future for biomaterial industry.

Acknowledgements This study was supported by National Natural Science Foundation of China (51272176, 11075116), National Basic Research Program of China (973 Program, 2012CB933600), and Youth Foundation of Tianjin Normal University (52XQ1204). The Key Project of Tianjin Municipal Natural Science Foundation of China (13JCZDJC33900) supported partly the design and synthesis of graphene and NH₂ ion implanted graphene (G-NH₂). We appreciate Minsi Li, undergraduate student in School of Chemistry and Materials Science, University of Science and Technology of China, for her kind idea and contribution to synthesis of graphene and NH₂ ion implanted graphene.

References

- Bermudez E, Mangum JB, Wong BA, Asgharian B, Hext PM, Warheit DB, Everitt JI. Pulmonary responses of mice, rats, and hamsters to subchronic inhalation of ultrafine titanium dioxide particles. *Toxicol Sci*. 2004;77:347–57.
- Pan B, Cui D, Ozkan CS, Ozkan M, Xu P, Huang T, Liu F, Chen H, Li Q, He R, Gao F. Effects of carbon nanotubes on photoluminescence properties of quantum dots. *J Phys Chem C*. 2008;112:939–44.
- Cui D, Tian F, Ozkan CS, Wang M, Gao H. Effect of single wall carbon nanotubes on human HEK293 cells. *Toxicol Lett*. 2005;155:73–85.
- Lam CW, James JT, McCluskey R, Hunter RL. Pulmonary toxicity of single-wall carbon nanotubes in mice 7 and 90 days after intratracheal instillation. *Toxicol Sci*. 2004;77:126–34.
- Wang Z, Ruan J, Cui D. Advances and prospect of nanotechnology in stem cells. *Nanoscale Res Lett*. 2009;4:593–605.
- Liu Y, Yu D, Zeng C, Miao Z, Dai L. Biocompatible graphene oxide based glucose biosensors. *Langmuir*. 2010;26:6158–60.
- Peng C, Hu W, Zhou Y, Fan C, Huang Q. Intracellular imaging with a graphene based fluorescent probe. *Small*. 2010;6:1686–92.
- Sun X, Liu Z, Welsher K, Robinson JT, Goodwin A, Zaric S, Dai H. Nano-graphene oxide for cellular imaging and drug delivery. *Nano Res Lett*. 2008;1:203–12.
- Liu Z, Robinson JT, Sun X, Dai H. PEGylated nano-graphene oxide for delivery of water insoluble cancer drugs. *J Am Chem Soc*. 2008;130:10876–7.
- Hu W, Peng C, Luo W, Lv M, Li X, Li D, Huang Q, Fan C. Graphene based antibacterial paper. *ACS Nano*. 2010;4:4317–23.
- Akhavan O, Ghaderi E. Toxicity of graphene and graphene oxide nanowalls against bacteria. *ACS Nano*. 2010;4:5731–6.
- Yang K, Zhang S, Zhang G, Sun X, Lee ST, Liu Z. Graphene in mice: ultrahigh in vivo tumor uptake and efficient photo-thermal therapy. *Nano Lett*. 2010;10:3318–23.
- Robinson JT, Tabakman SM, Liang Y, Wang H, Casalongue SH, Vinh D, Dai H. Ultrasmall reduced graphene oxide with high near-infrared absorbance for photothermal therapy. *J Am Chem Soc*. 2011;133:6825–31.
- Heo C, Yoo J, Lee S, Jo A, Jung S, Yoo H, Lee YH, Suh M. The control of neural cell-to-cell interactions through non-contact electrical field stimulation using graphene electrodes. *Biomaterials*. 2011;32:19–27.
- Wang K, Ruan J, Song H, Zhang J, Wo Y, Guo S, Cui D. Biocompatibility of graphene oxide. *Nanoscale Res Lett*. 2011;6:4317–23.
- Ryoo SR, Kim YK, Kim MH, Min DH. Behaviors of NIH-3T3 fibroblasts on graphene/carbon nanotubes: proliferation, focal adhesion, and gene transfection studies. *ACS Nano*. 2010;4:6587–98.
- Chang Y, Yang ST, Liu JH, Dong E, Wang Y, Cao A, Liu YF, Wang HF. In vitro toxicity evaluation of graphene oxide on A549 cells. *Toxicol Lett*. 2010;200:201–10.

18. Shan C, Yang H, Han D, Zhang Q, Ivaska A, Niu L. Water-soluble graphene covalently functionalized by bio-compatible poly-L-lysine. *Langmuir*. 2009;25:12030–3.
19. Luo J, Cote LJ, Tung VC, Tan ATL, Goins PE, Wu J, Huang J. Graphene oxide nanocolloids. *J Am Chem Soc*. 2010;132:17667–9.
20. Kim YJ, Abe Y, Yanaglura T, Park KC, Shimizu M, Iwazaki T, Nakagawa S, Endo M, Dresselhaus MS. Easy preparation of nitrogen-enriched carbon materials from peptides of silk fibroins and their use to produce a high volumetric energy density in supercapacitors. *Carbon*. 2007;45:2116–25.
21. Hulicova-Jurcakova D, Kodama M, Shiraishi S, Hatori H, Zhu ZH, Lu GQ. Nitrogen-enriched nonporous carbon electrodes with extraordinary supercapacitance. *Adv Funct Mater*. 2009;19: 1800–9.
22. Yang XQ, Wu DC, Chen XM, Fu RW. Nitrogen enriched nanocarbons with a 3-D continuous mesopore structure from polyacrylonitrile for supercapacitor application. *J Phys Chem C*. 2010;114:8581–6.
23. Jurewicz K, Babel K, Ziolkowski A, Wachowska H. Ammoniation of active carbons for improvement of supercapacitor characteristics. *Electrochim Acta*. 2003;48:1491–8.
24. Jurewicz K, Babel K, Pietrzak R, Delpeux S, Wachowska H. Capacitance properties of multi-walled carbon nanotubes modified by activation and ammoniation. *Carbon*. 2006;44:2368–75.
25. Pietrzak R, Jurewicz K, Nowicki P, Babel K, Wachowska H. Nitrogen-enriched bituminous coal-based active carbons as materials for supercapacitors. *Fuel*. 2010;89:3457–67.
26. Guo HL, Gao QM. Boron and nitrogen co-doped porous carbon and its enhanced properties as supercapacitor. *J Power Sources*. 2009;186:551–6.
27. Lai LF, Chen LW, Zhan D, Sun L, Liu JP, Lim SH, Poh CK, Shen ZX, Lin JY. One-step synthesis of G-NH₂ raphene from in situ graphene-oxide reduction and its improved electrochemical properties. *Carbon*. 2011;49:3250–7.
28. Singh SK, Singh MK, Kulkarni PP, Sonkar VK, Gracio JJA, Dash D. Amine-modified graphene: thrombo-protective safer alternative to graphene oxide for biomedical applications. *ACS Nano*. 2012;6:2731–40.
29. Li DJ, Cui FZ, Gu HQ. F ion implantation induced cell attachment on intraocular lens. *Biomaterials*. 1999;20:1889–96.
30. Venkatesan T, Dynes RC, Wilkens B, White AE, Gibson JM, Hamm R. Comparison of conductivity produced in polymers and carbon films by pyrolysis and high energy ion irradiation. *Nucl Instrum Meth B*. 1984;1:599–604.
31. Koh SK, Choi KW, Cho JS, Song SK, Kim YM, Jung HJ. Ar⁺ ion irradiation in oxygen environment for improving wettability of polymethylmethacrylate. *J Mater Res*. 1996;11:2933–9.
32. Wang GH, Pan GQ, Dou L. Proton beam modification of isotactic polypropylene. *Nucl Instrum Meth B*. 1987;27:410–6.
33. Wang GH, Li XJ, Zhu YZ, Liu QS, Hu NX, Gu XS, Wang Q, Yu RX, Wang TJ. Radiation effects on polyethylene and polypropylene by electrons and protons. *Nucl Instrum Meth B*. 1985;7: 497–500.
34. Licciardello A, Fragala ME, Foti G, Compagnini G, Puglisi Q. Ion beam effects on the surface and on the bulk of thin films of polymethylmethacrylate. *Nucl Instrum Meth B*. 1996;116: 168–72.
35. Lee HJ, Park J, Yoon OJ, Kim HW, Lee DY, Kim DH, Lee WB, Lee NE, Bonventre JV, Kim SS. Amine-modified single-walled carbon nanotubes protect neurons from injury in a rat stroke model. *Nat Nanotechnol*. 2011;6:121–5.
36. Lee W, Parpura V. Wiring neurons with carbon nanotubes. *Front Neuroeng*. 2009;2:1–3.
37. Geng DS, Yang SL, Zhang Y, Yang JL, Liu J, Li RY, Sham TK, Sun XL, Ye S, Knights S. Nitrogen doping effects on the structure of graphene. *Appl Surf Sci*. 2011;257:9193–8.
38. Grinnell F, Feld MK. Fibronectin adsorption on hydrophilic and hydrophobic surfaces detected by antibody binding and analyzed during cell adhesion in serum-containing medium. *J Biol Chem*. 1982;257:4888–93.
39. Lu DR, Park K. Effect of surface hydrophobicity on the conformational changes of adsorbed fibrinogen. *J Colloid Interface Sci*. 1991;144:271–81.
40. Zhao ML, Li DJ, Yuan L, Yue YC, Liu H, Sun XL. Differences in cytocompatibility and hemocompatibility between carbon nanotubes and nitrogen-doped carbon nanotubes. *Carbon*. 2011;49: 3125–33.
41. Akasaka T, Yokoyama A, Matsuoka M, Hashimoto T, Watari F. Thin films of single-walled carbon nanotubes promote human osteoblastic cells (Saos-2) proliferation in low serum concentrations. *Mater Sci Eng, C*. 2010;30:391–9.
42. Magrez A, Kasas S, Salicio V, Pasquier N, Seo JW, Celio M, Catsicas S, Schwaller B, Forro L. Cellular toxicity of carbon-based nanomaterials. *Nano Lett*. 2006;6:1121–5.
43. Yu X, Cai H, Zhang W, Li X, Pan N, Luo Y, Wang X, Hou JG. Tuning chemical enhancement of SERS by controlling the chemical reduction of graphene oxide nanosheets. *ACS Nano*. 2011;5:952–8.
44. Sanchez VC, Jachak A, Hurt RH, Kane AB. Biological interactions of graphene family nanomaterials: an interdisciplinary review. *Chem Res Toxicol*. 2012;25:15–34.
45. Motlagh D, Yang J, Lui KY, Webb AR, Ameer GA. Hemocompatibility evaluation of poly (glycerol-sebacate) in vitro for vascular tissue engineering. *Biomaterials*. 2006;27:4315–24.